



Published in final edited form as:

Cell Rep. 2021 July 20; 36(3): 109416. doi:10.1016/j.celrep.2021.109416.

Phosphorylated WNK kinase networks in recoded bacteria recapitulate physiological function

Paula Schiapparelli^{1,9}, Natasha L. Pirman^{2,3,9}, Kyle Mohler^{2,3}, Pierre A. Miranda-Herrera¹, Natanael Zarco¹, Onur Kilic⁴, Chad Miller⁵, Sagar R. Shah⁴, Svetlana Rogulina^{2,3}, William Hungerford⁶, Laura Abriola⁶, Denton Hoyer⁶, Benjamin E. Turk⁵, Hugo Guerrero-Cázares¹, Farren J. Isaacs^{3,7,8}, Alfredo Quiñones-Hinojosa¹, Andre Levchenko^{2,7,8}, Jesse Rinehart^{2,3,10,*}

¹Department of Neurologic Surgery, Mayo Clinic, Jacksonville, FL 32224, USA

²Department of Cellular & Molecular Physiology, Yale School of Medicine, New Haven, CT 06520, USA

³Systems Biology Institute, Yale University, West Haven, CT 06516, USA

⁴Department of Biomedical Engineering, Johns Hopkins University, Baltimore, MD 21205, USA

⁵Department of Pharmacology, Yale University School of Medicine, New Haven, CT 06520, USA

⁶Yale Center for Molecular Discovery, Yale University, West Haven, CT 06516, USA

⁷Department of Molecular, Cellular & Developmental Biology, Yale University, New Haven, CT 06520, USA

⁸Department of Biomedical Engineering, Yale University, New Haven, CT 06511, USA

⁹These authors contributed equally

¹⁰Lead contact

SUMMARY

Advances in genetic code expansion have enabled the production of proteins containing site-specific, authentic post-translational modifications. Here, we use a recoded bacterial strain with an expanded genetic code to encode phosphoserine into a human kinase protein. We directly encode phosphoserine into WNK1 (with-no-lysine [K] 1) or WNK4 kinases at multiple, distinct sites, which produced activated, phosphorylated WNK that phosphorylated and activated SPAK/OSR

This is an open access article under the CC BY-NC-ND license (<http://creativecommons.org/licenses/by-nc-nd/4.0/>).

*Correspondence: jesse.rinehart@yale.edu.

AUTHOR CONTRIBUTIONS

Conceptualization, P.S., N.L.P., F.J.I., D.H., A.Q.-H., A.L., and J.R.; formal analysis, J.R., N.L.P., P.S., and D.H.; funding acquisition, J.R., F.J.I., A.L., A.Q.-H., and B.E.T.; investigation, N.L.P., P.S., P.A.M.-H., S.R.S., S.R., K.M., N.Z., O.K., C.M., W.H., L.A., D.H., and H.G.-C.; methodology, J.R., F.J.I., A.L., A.Q.-H., D.H., W.H., and L.A.; resources, N.Z., P.A.M.-H., H.G.-C., J.R., F.J.I., A.L., A.Q.-H., and D.H.; supervision, P.S., J.R., and A.Q.-H.; visualization, J.R., N.L.P., P.S., O.K., and K.M.; writing – original draft, J.R., N.L.P., K.M., and P.S.; writing – review & editing, J.R. and P.S.

DECLARATION OF INTERESTS

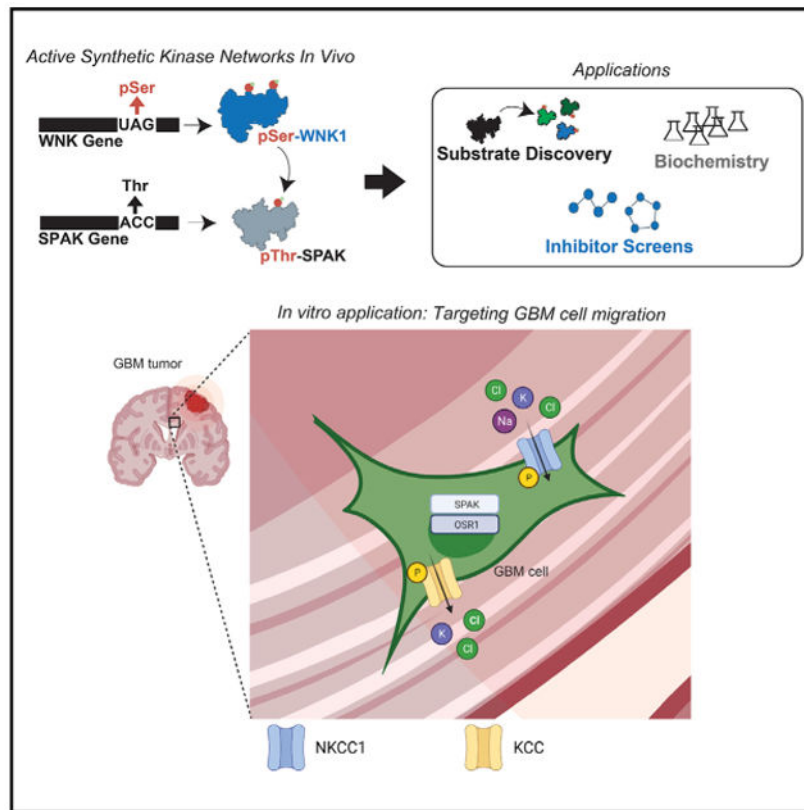
All authors declare no competing interests.

SUPPLEMENTAL INFORMATION

Supplemental information can be found online at <https://doi.org/10.1016/j.celrep.2021.109416>.

kinases, thereby synthetically activating this human kinase network in recoded bacteria. We used this approach to identify biochemical properties of WNK kinases, a motif for SPAK substrates, and small-molecule kinase inhibitors for phosphorylated SPAK. We show that the kinase inhibitors modulate SPAK substrates in cells, alter cell volume, and reduce migration of glioblastoma cells. Our work establishes a protein-engineering platform technology that demonstrates that synthetically active WNK kinase networks can accurately model cellular systems and can be used more broadly to target networks of phosphorylated proteins for research and discovery.

Graphical abstract



In brief

Schiapparelli et al. describe a protein-engineering platform technology to synthetically activate the WNK/SPAK/OSR1 kinase network. Using this approach, they identify biochemical properties of WNK and SPAK kinases along with small-molecule inhibitors for SPAK. Cellular systems, both *in vitro* and *in vivo*, translate findings from the engineered kinase network.

INTRODUCTION

Protein phosphorylation is among the most abundant and wellstudied post-translational modifications (PTMs) that control the function of individual proteins and protein networks. However, as the list of phosphorylation sites has grown rapidly, our knowledge of their function has concurrently dwindled (Needham et al., 2019). This lack of functional

annotation is, in part, due to the lack of techniques permitting the site-specific synthesis of authentically phosphorylated proteins. Although bacterial expression systems are a gold standard for protein production, there are barriers to expression of active, post-translationally modified human proteins. Heterologous systems typically lack the signaling networks required to activate kinases. Often the precise mechanisms of kinase activation, mostly via phosphorylation, are poorly understood and constrain heterologous production of active phosphorylated proteins. Although acidic amino acid substitutions of aspartate or glutamate for phosphoserine are used to mimic the effect of phosphorylation, they often fail to recapitulate biological activity. We have overcome these major barriers by enabling the heterologous expression of authentically phosphorylated proteins using a genomically recoded strain of *E. coli* (Isaacs et al., 2011; Lajoie et al., 2013) paired with a phosphoserine orthogonal translation system (pSerOTS) (Park et al., 2011; Pirman et al., 2015). The genomically recoded strain of *E. coli* has the UAG stop codon function eliminated from its genetic code through the reassignment of all UAG to UAA codons and the deletion of release factor 1. This recoded *E. coli* has the UAG codon available for reassignment to a new amino acid. To assign UAG to phosphoserine, the pSerOTS uses a phosphoseryl-tRNA synthetase (pSerRS) to aminoacylate pSer onto a UAG-decoding tRNA^{pSer} and an engineered elongation factor Tu (EF-pSer) to deliver pSer-tRNA^{pSer} to the ribosome, thus allowing expression of recombinant proteins with site-specific authentic phosphorylation (Figure 1A). These synthetic biology tools have provided solutions for the generation and analysis of post-translationally modified proteins (Barber and Rinehart, 2018).

In this work, we aimed to endow a human kinase network with authentic, programmable phosphorylation sites to provide an active network as a discovery platform (Figure 1A). We chose to genetically encode pSer in the first kinase of a cascade to control its activity in the absence of upstream regulators. We then co-expressed the downstream target of the first kinase to produce an active kinase pair. We selected the WNK (with-no-lysine [K]) kinase and SPAK/OSR1 (STE20/SPS1-related proline/alanine-rich kinase/oxidative stress response) kinase pair for this work because many of the critical phosphorylation sites that impart network control have been defined (Moriguchi et al., 2005; Rafiqi et al., 2010; Thastrup et al., 2012; Vitari et al., 2005, 2006; Dowd and Forbush, 2003; Piechotta and Delpire, 2002). However, precise control over the kinase pair *in vivo* has not been achieved, and a programmable WNK-SPAK/OSR1 network would be a useful platform for discovery.

The WNK-SPAK/OSR1 network plays an essential role in the maintenance of cell volume by controlling the phosphorylation of ion co-transporters, particularly NKCC1 (Na⁺-K⁺-Cl⁻ co-transporter 1) and KCC (potassium chloride cotransporter) (Dowd and Forbush, 2003; Piechotta and Delpire, 2002). More recently the WNK-SPAK/OSR1 network has been implicated in the regulation of T cell migration and adhesion *in vivo* (Köchler et al., 2016) and promoting tumorigenesis and cell invasion in hepatocarcinoma (Sie et al., 2020). Glioblastoma multiforme (GBM), one of the most aggressive brain cancers, manipulates cellular volume, focal adhesions, and the actin cytoskeleton through alterations in the activity of WNK-SPAK-controlled ion co-transporters to facilitate migration (Garzon-Muvdi et al., 2012; Schiapparelli et al., 2017). GBM tissues and derived cell lines have shown abundant expression of WNK1–4, SPAK, and OSR1, and stable knockdown of WNK3 and OSR1 lead to decreased GBM cell migration *in vitro* (Zhu et al., 2014; Haas et al., 2011).

Taken together, these observations suggest that inhibition of kinases in the WNK-SPAK regulatory network and subsequent reduction in ion co-transporter activity may provide an effective strategy to prevent infiltration of GBM cells and possibly halt tumor growth.

We found that genetically encoded pSer imparted exquisite control over WNK1 activity. Furthermore, active WNK1 could phosphorylate SPAK and OSR1 at the canonical activation sites in our bacterial system, thereby producing an active WNK-SPAK/OSR network containing on-target, authentic phosphorylation sites. The programmable WNK-SPAK pathway enabled substrate profiling of active SPAK and a screen for small-molecule SPAK kinase inhibitors. A kinase inhibitor that targeted the synthetic WNK-SPAK pathway also inhibited NKCC and KCC phosphorylation in cells, which resulted in acute cell volume reduction. The same small molecule reduced cell migration in GBM cells and recapitulated on-target effects of SPAK/OSR1 double knockdown with short hairpin RNAs (shRNAs). This work establishes a programmable system for the complete WNK/OSR/SPAK network and provides a potential path toward constructing synthetic mammalian phosphoprotein networks more broadly as scaffolds for drug discovery.

RESULTS

Recombinant phosphorylated WNK1 reconstitutes a native WNK-SPAK signaling network

We expressed multiple forms of phosphorylated human WNK1: S382 (1SP) and S378/S382 (2SP) with (WNK1,1–661) and without (WNK1,1–483) its native autoinhibitory domain (AID) using the pSerOTS in the genomically recoded *E. coli* strain (C321). A) (Figure S1A). Additionally, we expressed full-length SPAK either on its own or co-expressed with phosphorylated WNK1 for downstream evaluation of WNK1 activity (Figures 1 and 2). The kinases were purified using affinity chromatography, and phosphoserine incorporation was confirmed using a phospho-specific antibody recognizing S^P382 WNK1 (Figure S1A) and by mass spectrometry (Figure S2), confirming that SPAK was phosphorylated at its physiologically relevant positions. Kinase activity was measured with an N-terminal fragment of the ion co-transporter NKCC1 and a phospho-specific antibody (Flemmer et al., 2002). When expressed separately, neither S^P382-WNK1 nor SPAK could phosphorylate the NKCC1 substrate (Figure 1B, lanes 1–3). However, robust NKCC1 phosphorylation was observed when SPAK was co-expressed with any of the four S^P-WNK1 constructs (Figure 1B, lanes 4–7). As expected, NKCC1 phosphorylation was abolished when kinase dead (KD) WNK1 or KD SPAK was used in the system (Figure 1B, lanes 8 and 9).

Genetically encoded pSer yields more active kinases than phosphomimetic amino acids at the key physiological activation sites

Since prior studies have used a glutamate substitution (T233E) in an attempt to mimic SPAK phosphorylation and circumvent the need for WNK1 activation (Rafiqi et al., 2010; Richardson and Alessi, 2008; Vitari et al., 2005, 2006), we next aimed to rigorously compare this method with the use of our highly active, recombinant WNK-SPAK system. We thus evaluated co-expressed WNK1-SPAK variants through *in vitro* kinase reactions with and without MO25 α (a known enhancer of SPAK activity) by evaluating NKCC1 phosphorylation by ³²P autoradiography (Figures 1C, 2A, and 2C) (Filippi et al., 2011;

Grimm et al., 2012). Unmodified SPAK expressed in bacteria had no detectable activity either with or without MO25 α , while the phosphomimetic SPAK (T233E) possessed low activity with a small but reproducible enhancement in the presence of MO25 α (Figure S1B). In contrast to both unmodified and SPAK-T233E, each S^PWNK1-SPAK preparation (either S^P382 WNK1 or S^P378/S^P382 WNK1) was more active than the phosphomimetic glutamate substitutions with substantially enhanced activity in the presence of MO25 α (Figures 1C and 2C). Unlike the 1S^PWNK1-SPAK variants, the 2S^PWNK1-SPAK variants had equivalent activity with or without their AID (Figure 1C). KD WNK1 was inactive with or without its AID and did not undergo autophosphorylation or subsequent SPAK activation. These results show that the network activity is exquisitely controlled by the genetically encoded pSer in WNK1. Consistent with previous studies (Xu et al., 2002), WNK1 containing the AID had minimal activity, and WNK1 without the AID had nearly 1.5-fold more activity. This shows that WNK1 proteins containing the AID prevent autophosphorylation and limit their use in a synthetic network. Similarly, WNK1 with aspartate phosphomimetic substitutions showed minimal kinase activity with the AID. Although the phosphomimetic WNK1 variants gained a modest SPAK-activating function without their AID (Figure 1C, WNK1-483 1D), they still had less activity when compared to the wild-type (WT) without the AID (Figure 1C, WNK1-483 WT), confirming previous reports, which showed that phosphomimetic WNK1 variants had less activity than autophosphorylated WT WNK1 (Xu et al., 2002). However, the genetically encoded 1S^P and 2S^P WNK1 variants produced the most active SPAK. Furthermore, 1S^P WNK1 gained substantial activation without the AID, indicating that the AID still modulated the activation of the second S^P WNK1 site through inhibiting autophosphorylation (Figure 1C, WNK1-166 1S^P versus WNK1-438 1S^P). In comparison, the 2S^P WNK1 variants showed similar levels of increased kinase activity with or without the AID. These experiments confirm that both phosphoserine at S382 and S378/S382 in the canonical activation loop of WNK1 are sufficient for WNK1 activation and that autoinhibitory mechanisms can be overcome by genetically encoding pSer. Furthermore, direct synthesis of the pSer WNK1, without an upstream kinase, proves that the two activation site phosphoserines are sufficient to block autoinhibition and highlights a distinct advantage of the system to provide mechanistic insight.

To demonstrate the flexibility of the synthetic network, we tested combinations of WNK1, WNK4, SPAK, and OSR1 since these four different kinases comprise many WNK kinase networks *in vivo* (Vitari et al., 2005, 2006) (Figure 2). WNK4 was inactive without genetically encoded pSer and, similar to WNK1, could robustly activate SPAK. WNK1 was also able to activate both OSR1 and SPAK (Figure 2B). All forms of active WNK1 also showed productive interactions with the co-factor MO25 α (Figure 2C). This protein is an important modulator of network function *in vivo*, and these results show that the reconstituted network can respond to co-factors. Taken together, these data demonstrate our ability to produce catalytically active human WNK kinase networks that can be used in different combinatorial arrangements that maintain physiologically relevant function.

S^PWNK1-activated SPAK conforms to known substrates

Our ability to generate authentically phosphorylated SPAK provided the opportunity to profile the sequence preference of its substrates and generate a SPAK kinase motif. To

identify a SPAK kinase motif, we performed a high-throughput *in vitro* kinase assay using a published positional scanning peptide library (PSPL) (Hutti et al., 2004). Quantified data from the PSPL (Figure 3A, left panel) were used to generate a sequence logo that illustrates the amino acid preferences at each position relative to the phosphorylation site (Figure 3A, right panel). Comparison of the results from the peptide screen to known phosphorylation sites on canonical substrates suggests strong preferences for tyrosine and histidine residues at the -3 and -2 positions, for hydrophobic residues at the +1 position, and for a Thr phosphoacceptor residue (Figure 3B). These data can be used to identify kinase-specific substrate preference even within closely related kinases. For example, our SPAK motif is distinct from a closely related STE20 kinase family, MST4, which has a strong preference for lysine and arginine residues at the +2, +3, and +4 positions (Miller et al., 2008). Our *in vitro* SPAK kinase motif resembled *in vivo* SPAK substrate phosphorylation sites (Rinehart et al., 2009) (Figure 3B). For example, the PSPL motif shows -3 and -2 tyrosine enrichment that suggests substrates could contain either -3 or -2 tyrosine. Both examples are found in the *in vivo* SPAK substrates for where NCC proteins have a -2 tyrosine in the second SPAK phosphorylation site (GYNpTIDV) while NKCC and KCC proteins have -3 tyrosine in their first SPAK phosphorylation site (TYERpTL). These results show further support that kinase networks activated with genetically encoded pSer can recapitulate physiological function.

Small-molecule inhibitor ELISA screen identifies potential SPAK inhibitors

Our approach offers a unique and physiologically relevant platform to use authentically phosphorylated kinase networks to identify small-molecule kinase inhibitors. Combining our S^PWNK1-SPAK with an ELISA-based assay to measure NKCC1 phosphorylation, we performed a screen of 360 compounds from the GlaxoSmithKline (GSK) published protein kinase inhibitor set (PKIS-1) (Dranchak et al., 2013) to identify potential SPAK inhibitors (Figure 3C). This library was a subset of a larger library pre-screened to identify ATP-competitive kinase inhibitors. We identified seven compounds (inhibitor [Inh.] A/B, C, D, E, F, G), which reduced NKCC1 phosphorylation 34%–58% at a concentration of 27 μM (Figure S3A). Four distinct chemotypes were apparent out of the seven identified. Two happened to be identical from different manufacturers (Inh. A/B and Inh. H, Figure S3B), three others fell into the same chemotype, and two additional compounds were unique. One hit from each chemotype (Inh. B, C, D, E) identified in the ELISA-based screen was further evaluated for dose-dependent inhibition of both NKCC1 and KCC phosphorylation. Careful rescreening of these hits identified compounds C and E as false positives (Figure 3D).

Prior work has shown that hypo- and hyper-osmotic conditions can activate or deactivate the WNK-SPAK-NKCC1 signaling cascade, respectively (Zagórska et al., 2007). We evaluated these conditions in a mouse distal convoluted tubule cell line (mDCT15) to establish the upper and lower limits of signal detection for the T^PNKCC1 immunoblot assay (Figure S3D). We monitored NKCC1 phosphorylation under hyper- and hypo-osmotic conditions to evaluate the degree of SPAK inhibition in the presence of the putative inhibitors (Figure 3E). The vehicle controls showed a prominent T^PNKCC1 signal as expected, while cells treated with the compounds yielded inhibitory effects consistent with the *in vitro* kinase assay. As a final validation, SPAK inhibitor A was resynthesized and named YU239252 (herein referred to as YU252) and analyzed by Fourier transform ion cyclotron resonance tandem

mass spectrometry (FTICR MS/MS) (Figure S4). The half-maximal inhibitory concentration (IC_{50}) of YU252 was determined to be 8.23 μ M at 10 μ M ATP using our *in vitro* SPAK ELISA assay (Figure S5A). These results demonstrate the utility kinase networks activated with genetically encoded pSer for standard HTS hit validation workflows.

The GSK PKIS library annotates YU252 and another compound, Inh. H, as similar chemotypes and potent VEGFR2/Tie-2 inhibitors. Interestingly, Inh. H was not identified in our initial ELISA screen as a SPAK inhibitor (Figure S3B). To validate that Inh. H did not inhibit SPAK, we performed an *in vitro* kinase assay comparing a dilution series of YU252 and Inh. H (Figure S3C). These data revealed that, although YU252 and Inh. H reportedly both inhibit VEGFR2/Tie-2 with similar potency, the two compounds do not have the same inhibitory effect on SPAK. Additionally, we also examined both YU252 and Inh. H effects on NKCC1 phosphorylation in the mDCT15 cell line at two different concentrations (Figure S5B). YU252 caused an almost complete reduction in NKCC1 phosphorylation. However, at the same concentrations Inh. H did not inhibit SPAK to the same extent as did YU252. This result suggested that inhibition of VEGFR2 or Tie-2 was not the cause for the reduction in NKCC1 phosphorylation. To further explore the putative involvement of VEGFR2 or Tie-2 signaling, we compared the effect of YU252 to that of a potent commercially available VEGFR2/Tie-2 inhibitor, cabozantinib malate (XL-184) (Figures 4A and 4B). Based on the known physiology of the ion co-transporters' role in maintaining ion homeostasis, we hypothesized that upon inhibiting SPAK, phosphorylation of the ion co-transporters would decrease over time without the need of any upstream hyper- or hypo-osmotic triggers (Figure 4B). Indeed, YU252 caused a noticeable reduction in NKCC1 phosphorylation; however, at the same dose (6-fold higher than its known pIC_{50} for VEGFR2), XL-184 had no discernable effect on NKCC1 phosphorylation. Based on the time course results, we hypothesized that as the ion co-transporters become inactivated, cells could undergo regulatory volume decrease and shrink overtime. We evaluated the response of mDCT15 cells by microscopic imaging after incubation with YU252, XL-184, or vehicle control (Figures 4A, S5D, and S5E). The results showed that YU252 indeed caused a cell volume decrease in these cells, while neither XL-184 nor vehicle had any detectable effect over the time monitored. These data show that YU252-mediated SPAK inhibition results in a reduction of NKCC1 phosphorylation and cell volume decrease, as anticipated. Inhibitor B was further evaluated with a dilution series to determine the potency in the mDCT15 cells (Figure S5C). Similar to the initial *in vivo* assay, inhibitor concentrations of 40 μ M completely blocked NKCC1 phosphorylation. In doseresponse assays, these compounds had approximately 50% inhibition at 10 μ M, and no inhibitory effect at concentrations below ~625 nM.

YU252 decreases ion co-transporter activity and inhibits migration in glioblastoma cells

To migrate through the brain parenchyma, GBM cells may rely on volume alterations facilitated by ion co-transporters, particularly NKCC1 and KCC, involving WNK and SPAK/OSR1 (the only known kinases responsible for directly activating these ion co-transporters *in vivo*). To test the effects of YU252 in GBM migration, we first confirmed the expression NKCC1 and SPAK in a panel of patient-derived GBM cell lines by immunoblotting (Figure S6A). We next tested SPAK pathway inhibition by monitoring the

physiological SPAK substrates NKCC1 and KCC4 (Rinehart et al., 2009) and showed that YU252 inhibited phosphorylation of endogenous NKCC1 and KCC4 in three different GBM cell lines, in a dose-dependent manner (Figures S6C-S6E). To assess the effect of YU252 on cell migration, we used an established quasi-3D migration assay employing a tissue-mimetic nanopatterned substrate (Garzon-Muvdi et al., 2012; Smith et al., 2016). This artificial, topographically structured surface permits accurate, single-cell quantification of cell motility (Figure 4C). We assayed migration speed of GBM cell lines in the presence of YU252 versus a vehicle control (Figures 4C, 4D, and S6F-S6H). We found that YU252 reduced the migration speed in a concentration-dependent manner (Figure 4D). Assessment of individual cell speed values in the GBM heterogeneous population revealed that the speed of most cells was retarded when compared to the vehicle control (Figures 4C and S6B; Videos S1 and S2). Evaluation of the average speed revealed that YU252 reduced the average migration speed in all of the GBM cell lines tested (Figures S6F-S6H). These results indicate that YU252, by reducing both NKCC1 and KCC phosphorylation, can dramatically decrease GBM cell migration. To investigate whether cell migration is driven by SPAK and OSR1, we constructed a single lentiviral vector encoding shRNAs designed to interfere with the expression of both proteins simultaneously (Figure 4E). We used our shRNAs in GBM965 and found that SPAK/OSR1 double knockdown (DKD) cells showed a pronounced decrease in cell migration (Figure 4E) and cell proliferation (Figure S7B) compared to the control (shEV). Next, we treated DKD and shEV cells with YU252 at different concentrations and analyzed NKCC1 phosphorylation and cell migration. NKCC1 phosphorylation was strongly reduced, accompanied by an approximated 50% decrease in NKCC1 protein expression (Figure S7A). We observed decreased migration in a concentration-dependent manner in all treated cells (Figure 4F). Given that baseline migration, proliferation, and NKCC1/KCC phosphorylation are greatly reduced in DKD cells, and are thus SPAK/OSR1-dependent as hypothesized, it was difficult to confirm the selectivity of YU252. However, both YU252 and DKD approaches target cell migration in the GBM lines tested, implying that a common pathway is targeted. YU252 selectivity screening done by us (Table S3) and others (GW770249A; <https://www.ebi.ac.uk/chembl/>) does not completely rule out off target activities that could explain the cellular effects of YU252. For example, we used higher concentrations of YU252 and a broader kinase panel than what was reported in the ChEMBL database and observed WNK kinase inhibition. More extensive structure-activity profiling in conjunction with followup selectivity screens could lead to a more potent and selective SPAK inhibitor. These types of studies could be carried out with our active WNK/SPAK-OSR1 network and potentially yield valuable further insights into the YU252 scaffold. In this study, we aimed to show that initial hit to lead identification could be faithfully translated to on-target cellular activity in support of the general utility of kinase networks activated with genetically encoded pSer.

YU252 inhibits glioblastoma proliferation and tumor growth in mice

Based on our time course inhibitor and migration assay results in GBM cells, we hypothesized that as the ion co-transporters become inactivated, cells can lose their ability to regulate volume and may undergo regulatory volume decrease, thereby shrinking over time. To test this hypothesis, we evaluated phenotypic changes in GBM1A cells incubated with YU252 or vehicle by microscopic imaging (Figures S7C and S7E). YU252 indeed caused a

reduction in cell volume, while cells treated with the vehicle alone had no detectable change (Figures S7C and S7E).

Because cell volume regulation through ion homeostasis is essential for cell division, we also analyzed the effect of SPAK inhibition on GBM proliferation. *In vitro* experiments with five GBM cell lines demonstrated a dose-dependent inhibition of proliferation in response to YU252 at 72hs (Figure S7D). To validate the inhibitor-mediated decrease in GBM proliferation *in vivo*, we established xenografts of GBM1A subcutaneously in nude mice. Systemic delivery of YU252 through daily intraperitoneal injections at low doses yielded significant inhibition of tumor growth, evaluated by bioluminescence (Figure 4G). GBM tumor formation in these assays was confirmed by H&E staining (Figure S7F). No changes in mouse weight were detected during treatment (Figure S7G), suggesting that YU252 displays low toxicity *in vivo*. It is important to highlight the fact that we saw the efficacy in tumor growth reduction using very low doses of the compound, even though the IC₅₀s for YU252 are in the 15 μ M range. Although these results demonstrate that YU252 can potentially be used to inhibit the WNK/SPAK-OSR1 network in GBM and limit tumorigenesis *in vivo*, further studies are required to establish the selectivity of YU252 *in vivo* or to define more potent and selective SPAK-OSR1 inhibitors. However, these findings are important validation steps demonstrating that insights gleaned from our active WNK/SPAK-OSR1 networks can translate to cellular and *in vivo* pathway analysis.

DISCUSSION

Despite their important role in cellular processes, efforts to understand the function of phosphorylation sites are hindered by the apparent complexity of the phosphoproteome. Many kinases are themselves activated by phosphorylation in their kinase domain activation loops, limiting the generation of active, recombinant kinases to the relatively small pool of kinases for which the upstream activating kinase is known. These limitations are highlighted in a large-scale study that showed that most human kinases expressed in bacteria are inactive (Szewczuk et al., 2009).

In this study, we utilized our synthetic biology platform to genetically encode protein phosphorylation to generate an active form of WNK1. Our active WNK could then phosphorylate and activate SPAK, which allowed us to identify a new SPAK kinase motif. Knowledge of the SPAK kinase motif can now provide insight into potential SPAK substrates that have yet to be identified. More broadly, our approach to use a heterologous expression system to generate an active, authentically modified human signaling network has the potential to unlock other important signaling pathways for substrate discovery and drug development. Since our approach utilizes human proteins expressed in bacterial cells, it will certainly not allow comprehensive access to all human proteins and pathways. Future efforts will require technology development focused on adding additional PTMs alone and in combination to begin to address some limitations.

Increasing our understanding of kinase functions and their underlying network connectivity opens new avenues for the development of therapeutics. Ion co-transporters are involved in the invasion of healthy brain tissue by migratory GBM cells (Cuddapah and

Sontheimer, 2011). This migratory activity is ultimately regulated through post-translational phosphorylation, mediated in part by the WNK kinases. WNK-SPAK activation has been found to enhance tumorigenesis in other types of tumors such as hepatocarcinoma (Sie et al., 2020) and cervical cancer (Chiu et al., 2014). In addition to this observation, the identification of causal mutations in WNK kinases, which result in hereditary forms of hypertension and hyperkalemia (Wilson et al., 2001), has guided the focus of many studies toward elucidation of the WNK signaling pathway and downstream substrates. As a result, WNK1 has been shown to regulate the STE20-related kinases SPAK/OSR1 (Moriguchi et al., 2005; Vitari et al., 2005), which, in turn, phosphorylate NKCC1 to facilitate cell-volume regulation (Giménez, 2006; Delpire and Gagnon, 2008). These studies, and many others, recognized that the WNK-SPAK signaling pathway comprised potential therapeutic targets for controlling aberrant activation of ion co-transporters (as in the case of GBM and hypertension), and some small-molecule inhibitors against these targets are beginning to emerge (Yamada et al., 2016; AlAmri et al., 2017; Kikuchi et al., 2015). In this study, we identify a small-molecule inhibitor derived from a screen against authentically modified SPAK, which, to date, has not been feasible. Our synthetic biology-based approach enabled the reconstruction of a mammalian network that was difficult to study and manipulate in its native context. This reductionism, combined with genetically encoded phosphorylation, created a rapid discovery and validation workflow that recapitulated physiological contexts, which further translated to successful application *in vitro*, into cells, and ultimately in an *in vivo* model system. We anticipate that similar strategies can now be built and tested for a long list of other difficult signaling networks that drive cancer physiology.

Limitations of the study

Further work is required to characterize the selectivity of YU252 by performing more in-depth profiling of inhibitor concentrations with *in vitro* and *in vivo* selectivity studies. YU252 inhibitor should be used with caution to study different aspects of WNK/SPAK/OSR1 biology. A more potent and selective inhibitor of SPAK/OSR1 could be produced with assays using our active WNK/SPAK/OSR1 network. Our study's goal was to show that initial hit to lead identification could be translated to on-target cellular activity, highlighting the innovation of genetically encoded pSer to produce druggable kinase networks.

STAR★METHODS

RESOURCE AVAILABILITY

Lead contact—Questions and requests for resources and reagents should be directed to the Lead Contact, Jesse Rinehart (jesse.rinehart@yale.edu).

Materials availability—YU252 inhibitor was resynthesized at Dr. Rinehart's laboratory. Synthesis protocols are available upon request and will be shared without restriction.

Data and code availability—This study did not generate datasets or codes.

EXPERIMENTAL MODEL AND SUBJECT DETAILS

Mouse distal convoluted tubule cell culture—Mouse distal convoluted tubule (mDCT15) cells were provided by Robert Hoover. (Emory) (Naguro et al., 2012). The mDCT15 cells were cultured in DMEM/Ham's F-12 media supplemented with 1% PSN and 5% FBS.

Patient-derived primary cell culture—Patient samples of glioma tissues were obtained, manipulated, and processed at the Johns Hopkins Hospital and the Mayo Clinic under the approval of the Institutional Review Board (IRB). GBM499 (age: 51, gender: male), GBM965 (age: 61, gender: female), GBM612 (age: 56, gender: female), GBM640 (age: 60, gender: female) primary cell lines were derived from intraoperative tissue samples from patients treated surgically for newly diagnosed glioblastoma multiforme without prior treatment. GBM1A (age: n/a, gender: male) cell line was obtained from Dr. Angelo Vescovi (Galli et al., 2004). Primary cells were cultured in Dulbecco's Modified Eagle Medium: Nutrient Mixture F-12, B27 serum free supplement (GIBCO), 20ng/mL epidermal growth factor (EGF), and 20ng/ml fibroblast-derived growth factor (FGF).

Mice and tumor xenograft—All animal protocols were approved by the Mayo Clinic Animal Care Institutional and Use Committee. 8-week male nude mice (athymic nude Foxn1nu, Jackson Laboratories, USA) were injected subcutaneously in the right flank with 2×10^6 primary glioblastoma cells (previously transduced with lentiviral particles to constitutively express GFP-Luciferase gene). Cells were re-suspended in 200 μ L of 1:1 mixture of DMEM F12:Matrigel matrix (Corning). Tumors were allowed to grow to 100 mm³ and then mice were randomized into individual treatment groups: the control vehicle group received PBS-0.025% DMSO (270 μ L /dose), and the treated group received 0.1 mg/kg YU252 in PBS-0.025% DMSO (270 μ L/dose). Daily treatment was given by intraperitoneal injections for 17 days. Tumor growth was assessed by Bioluminescence imaging.

METHODS DETAILS

Recombinant protein expression and purification

Protein expression: All *E. coli* strains used in this study were made chemically competent using a standard RbCl₂ method. EcAR7 cells were co-transformed with plasmids encoding for WNK1 and SPAK variants (Table S1). Combinations requiring SEP-activation of WNK1 were sequentially made chemically competent and the SEP-OTS plasmid was then transformed. Glycerol stocks were made from the transformed cells containing the correct antibiotic resistance. All cultures were started from a freshly streaked glycerol stock on LB agar plates with the appropriate combination of antibiotics and 0.08% glucose. Pre-cultures were inoculated with 5–20 colonies and grown overnight to confluency in LB media containing 0.08% glucose, and antibiotics. Pre-cultures were diluted to OD₆₀₀ of 0.15 AU into 100 mL LB media containing 0.08% glucose, antibiotics and 2 mM SEP and were incubated and shaken at 30°C, 230 rpm to an OD₆₀₀ 0.8 AU. Protein expression was then induced with 1 mM IPTG and expressed at 20°C, 230rpm for ~20–22 hr. After expression,

the cultures were harvested at 4000 g, 20 min, 4°C. All media was decanted, and pellets were stored at -80°C.

Protein purification: Thawed cell pellets were re-suspended in 5 mL of lysis buffer (50 mM Tris/HCl pH 7.4, 500 mM NaCl, 0.5 mM EDTA, 0.5 mM EGTA, 5 mM DTT, 1 mg/mL lysozyme, 50 mM NaF, 1 mM NaVO₄, 10% glycerol, Roche protease inhibitor tablet), and incubated on ice for 30 min, followed by sonication. The lysates were centrifuged at 22 000 g, 15 min, 4°C and the clarified lysate was transferred to a 15 mL falcon tube and centrifuged under the same conditions again to remove all remaining insoluble material. The clarified lysate was transferred to 200 µL bed volume of Glutathione Hi-Cap Matrix (QIAGEN Valencia, Ca) that was preequilibrated in lysis buffer and incubated at 4°C on a rotisserie shaker for 1 hr. The resin/lysate was centrifuged at 500 g, 5 min 4°C. The lysate was gently removed with ~200 µL of the lysate still above the resin, the lysate slurry mixture was re-suspended and transferred to a Pierce spin column (Thermo Scientific Waltham, Ma). The column was washed with 6 mL of GST column wash buffer (50 mM Tris/HCl pH 7.4, 500 mM NaCl, 0.5 mM EDTA, 0.5 mM EGTA, 5 mM DTT, 50 mM NaF, 1 mM NaVO₄, 10% glycerol). 200 µL of GST column elution buffer (50 mM Tris/HCl pH 7.4, 500 mM NaCl, 0.5 mM EDTA, 0.5 mM EGTA, 5 mM DTT, 50 mM NaF, 1 mM NaVO₄, 10% glycerol, 20 U GST-Prescission™ protease (GE Healthcare Pittsburgh, PA)) was added to the top of the resin. The column was capped and the resin/buffer slurry was incubated at 4°C on the rotisserie shaker overnight. The 200 µL elution was collected in a clean Eppendorf tube. Two additional 200 µL elutions were collected by adding GST column wash buffer to the top of the column via syringe without disturbing the resin. Expression and purity of each fraction was assessed by SDS-page.

The validated elutions were pooled, concentrated and buffer exchanged into protein storage buffer (50 mM Tris/HCl pH 7.4, 150 mM NaCl, 1mM DTT, 20% glycerol) using a 0.5 mL amicon ultra centrifugal filter (Millipore Billerica, MA) and the protein was stored at -20°C. The protein concentration was estimated by comparing known quantities of BSA standards on an SDS-page gel. The plasmid encoding for WT-SPAK was transformed into chemically competent BL21 (DE3) cells, and protein was expressed following the same protocol as above, with a few exceptions. Cells were grown at 37°C prior to induction, and no additives that are required for SEP-Tech were supplemented in the media.

Plasmid constructs—The following plasmids were generously provided from the Division of Signal Transduction (DSTT), Dundee: WT-WNK1 (DU6025), WT-SPAK (DU6040), Kinase Dead D212A-HA SPAK (DU6013), WT OSR1 (DU41905) and WT-MO25α (DU2945) in the pGEX-6P-1 backbone. All WNK and SPAK/OSR1 variants used in this study were made either by cloning, mutagenesis, or PCR and are derived from the DSTT plasmids following standard procedures. A zeocin antibiotic marker cassette was subcloned in place of the ampicillin antibiotic marker of the pGEX-6P-1 vector backbones for WT SPAK and WT OSR1 that were co-expressed with WNK1 variants. Each WNK1 variant derived from DU6025 is described in Table S1.

The pSerOTS was constructed by combining the pSepT and pKD-SepRS-EF5ep plasmids (Park et al., 2011) to create an all-in-one orthogonal translation system (OTS). The 250 bp

tRNA^{SEP} cassette was PCR amplified from the pSepT plasmid using primers tRNA^{SEP}-F (5'-ACC GCG GCC GCA AAA AAA ATC ctagctttcg-3') and tRNA^{SEP}-R (5'-AAA GCG GCC GCG CTT CTT TG agcgaac-3'). The PCR primers added NotI restriction sites to each end of the PCR product. The pKD-SepRS-EFSep plasmid was linearly digested with NotI and five copies of the tRNA^{SEP} cassette were ligated sequentially. N-terminal Strep-tagged human NKCC1 (Residues 1–260) was codon-optimized for *E. coli* and synthesized by Genewiz (South Plainfield, NJ). The gene fragment was subcloned into in pGEX-6P-1 using a 5' and 3' BamHI restriction site.

SPAK kinase assay measured by immunoblotting with T^PNKCC1—Kinase activity of purified WNK1, SPAK and co-expressed WNK1/SPAK variants were evaluated by measuring NKCC1 phosphorylation using the T^PNKCC1. Reactions containing different combinations of the following kinases and substrates were reacted for 1 hr at 37°C in immunoblotting kinase assay buffer (50 mM Tris/HCl pH 7.4, 150 mM NaCl, 1mM DTT, 20% glycerol, 10 mM MgCl₂, 0.2 mM ATP) at a final assay volume of 15 µL: 0.1–2.0 µM WNK1, 0.5–1 µM SPAK, and 5 µM strep-tagged NKCC1. The reaction was quenched with 15 µM of 2x Laemmli sample buffer, heated to 95°C for 5 min. Half of the quenched reaction was analyzed on two SDS-Page gels, and the samples were subjected to the immunoblotting procedure described above. Each membrane was cut at the 50 kDa protein marker and the bottom half of one membrane was immunoblotted for T^PNKCC1, and the other for Strep-tactin-HRP. The top half of the membranes were immunoblotted for Anti-SPAK, and WNK1 S^P382; respectively.

Antibodies—WNK1 S^P382 a rabbit polyclonal, phospho-specific antibody for S^P382 WNK1 was gifted from Richard Lifton, Yale University. To produce the antibody specific to WNK kinases phosphorylated at S382, the human WNK peptide acetyl-CGLATLKRASFAKS*VIG-cysteine (* phosphor-Ser), was coupled to keyhole limpet hemocyanin, and rabbits were immunized by the phosphopeptide (Covance Research Products). Pooled serum was depleted of nonspecific antibodies with the cognate nonphosphopeptide, and specific antibody was purified with the immunizing phosphopeptide. The antibody was used at a dilution of 1:10 000. T^PNKCC1 (R5), a rabbit polyclonal phospho-specific antibody for αphospho-NKCC (Flemmer et al., 2002) was gifted from Biff Forbush, Yale University and used at a dilution of 1:10 000 for both immunoblotting and ELISA. Strep-Tactin HRP conjugate was purchased from Iba-Life Sciences and used at a dilution of 1:50 000. Anti-SPAK a sheep polyclonal for total SPAK was purchased from the DSTT, Dundee used at a dilution if 1 µg/mL. Donkey Anti-Rabbit-HRP (DAR-HRP) and Donkey Anti-Sheep HRP (DASH-HRP) were purchased from Jackson ImmunoResearch and used at a dilution of 1:10,000.

Immunoblotting—Protein samples were subjected to electrophoresis on polyacrylamide gels and transferred to PVDF membranes. The membranes were incubated overnight in TBST blocking buffer containing 5% milk (w/v) (for the antibodies raised in sheep) or 3% BSA (w/v) (for all other antibodies). The membranes were immunoblotted with one of the following 1° antibodies in the appropriate blocking buffer for the denoted amount of time at RT: S^PWNK1 S382 (2 hr.), T^PNKCC1 (2 hr.), Strep-Tactin-HRP (1.5 hr.), or Anti-SPAK (1

hr). The membrane was then subjected to 3 washes in TBST for 5 min each, followed by the appropriate 2° antibody in blocking buffer for 1 hr at RT. The membranes were washed again 3 times in TBST for 5 min each. Signal was detected by enhanced chemiluminescence (Bio-Rad) imaged on a ChemiDoc XRS₊ CCD camera.

SPAK sample preparation for mass spectrometric analysis—Roughly 200 ng of the purified SPAK or co-expressed SPAK kinases were loaded on a 4%–12% Bis-Tris Invitrogen gel for SDS-page analysis. The gel was stained with Instant Blue™ (Expedeon, Harston Cambridgeshire, UK) for 1 hr. followed by destain in dH₂O overnight. The protein bands at the molecular weight corresponding to SPAK were excised and the gel pieces were cut into 1 mm cubes and put into clean 1.5 mL eppendorf tubes. Each sample was then sequentially washed for 10 min in 0.5 mL of each of the following solutions H₂O, 50% acetonitrile/H₂O, 0.1M NH₄HCO₃ and finally 50% acetonitrile/50 mM NH₄HCO₃ aspirating the liquid between each wash step. Next, the samples were “in gel” alkylated by adding 75 μL of 10 mM DTT/0.1M NH₄HCO₃ to each sample and incubating at 37°C for 20 min. The liquid was aspirated, and 75 μL of 50 mM iodoacetamide/0.1M NH₄HCO₃ was added to each sample and incubated at room temperature in the dark for 20 min. The liquid was aspirated, and the samples were further washed for 10 min in 0.5 mL 50 mM NH₄HCO₃ followed by 50% acetonitrile/50 mM NH₄HCO₃. The gel pieces were shrunk with 0.3 mL acetonitrile for 15 min. The liquid was aspirated, and the samples were dried by SpeedVac. The dried gel pieces were incubated with 50 μL of 25mM triethylammonium bicarbonate containing 5 μg/ml of Trypsin shaking at 30°C overnight.

Following the digestion, 50 μL of acetonitrile was added to the samples and they were incubated for 15 minutes. The supernatant was collected in a clean 1.5 mL Eppendorf tube and dried by SpeedVac. 100 μL of 50% acetonitrile/2.5% formic acid was added to the gel bands and incubated for 15 minutes. For mass spectrometry fingerprint analysis, the supernatant from the second extract was combined with the dried first extract then dried completely in a SpeedVac. The dried sample was stored at –20°C for analysis.

Mass spectrometric analysis—MS analysis was performed by LC-MS-MS using a linear ion trap-orbitrap hybrid mass spectrometer (Orbitrap-Classic, Thermo) equipped with a nanoelectrospray ion source (Thermo) and coupled to a Proxeon EASY-nLC system. Peptides were injected onto a Thermo (Part No. 160321) Acclaim PepMap100 reverse phase C₁₈ 3 μm column, 75 μm x 15cm, with a flow of 300 nl/min and eluted with a 45 min linear gradient of 95% solvent A (2% Acetonitrile, 0.1% formic acid in H₂O) to 40% solvent B (90% acetonitrile, 0.08% formic acid in H₂O), followed by a rise to 80%B at 48min. The instrument was operated with the “lock mass” option to improve the mass accuracy of precursor ions and data were acquired in the data-dependent mode, automatically switching between MS and MS-MS acquisition. Full scan spectra (m/z 340-1800) were acquired in the orbitrap with resolution R = 60,000 at m/z 400 (after accumulation to an FTMS Full AGC Target; 1,000,000; MSn AGC Target; 100,000). The 5 most intense ions, above a specified minimum signal threshold (5,000), based upon a low resolution (R = 15,000) preview of the survey scan, were fragmented by collision induced dissociation and recorded in the linear ion trap, (Full AGC Target; 30,000. MSn

AGC Target; 5,000). Multi-Stage-Activation was used to provide an MS3 scan of any parent ions showing a neutral loss of 48.9885, 32.6570, 24.4942, allowing for 2+, 3+ and 4+ ions respectively. The resulting MS3 scan was automatically combined with the relevant MS2 scan prior to data analysis. RAW files containing only CID data from the Orbitrap-Classic were analyzed both by using RAW2msm (Matthias Mann, Max-Planck Institute) followed by Mascot (www.matrixscience.com) searching against an in house database containing the relevant sequences and analyzed directly by using Proteome Discoverer 1.4 and phosphoRS 3.1 (Thermo), searching against the same database.

Kinase motif peptide screen—The peptide library (Kinase Substrates Library, Groups I and II, Anaspec, Inc.) has been described previously (Mok et al., 2010) and it consists of 198 peptide sets of the form Y-A-X-X-X-X-X-S/T-X-X-X-X-G-A-K-K(biotin), where, for each set, 8 of the 9 positions labeled X are degenerate mixtures of all 20 amino acids except serine, threonine, and cysteine. The other X position is fixed as one of the 20 standard amino acids or either phosphothreonine or phosphotyrosine, and the S/T represents an equimolar mixture of serine and threonine at the phosphorylation site. These 22 fixed amino acids at 9 positions comprise 198 peptide sets. The library also contains three peptides of the same form but with all the 9 X positions degenerate and only serine, threonine, or tyrosine at the phosphorylation site. These 201 peptide sets were assayed with SPAK in reaction buffer (50 mM Tris, pH 7.5, 10 mM MgCl₂, 1 mM EGTA in 0.1% tween) at final concentrations of 51 mM peptide library substrate, 10 nM SPAK or SPAK (kinase dead), 23 nM GST-MO25, 82 ng/μl BSA, and 45 μM ATP (including 0.027 μCi/μL [γ -³³P]ATP). The remaining transfer and washing steps of the assay were completed as previously described (Miller and Turk, 2016). The kinase dead control of SPAK prepared with active WNK gave no detectible signal (data not shown). After phosphorimager scanning (Molecular Imager FX Pro Plus, Bio-Rad), the median intensity of each spot was extracted. These values were then background corrected by subtracting the average signal of the 19 wells that contained kinase but no peptide. Background corrected data were then normalized by dividing them by the average intensity of all the 20 standard amino acids at the same fixed position. SPAK was assayed in duplicate, and the normalized data for each run were averaged. A Logo was created by inputting the positive values following log₂ transformations of these normalized, background corrected intensities into an online server (<http://www.benoslab.pitt.edu/cgi-bin/enologos/enologos.cgi>) (Workman et al., 2005).

SPAK kinase assay measured by ³²P radioactivity—30 nM SPAK, 2 μM GST-NKCC1 (DU6146), ± 1 μM GST-MO25α (DU30906) were reacted at 30°C in a Thermomixer at 1000 rpm from times ranging from 0–20 min in ³²P radioactive kinase assay buffer (50 mM Tris/HCl pH 7.4, 0.1 mM EGTA, 10 mM MgCl₂, 0.1 mM [³²P]-ATP (~200 c.p.m./pmol), 1 μM ovalbumin) at a final volume of 20 μL. The reactions were quenched with 20 μL of 2x Laemmli sample buffer, heated to 70°C for 10 min. The samples were subjected to electrophoresis on polyacrylamide gels, and stained with Instant Blue™ for 1 hr. followed by destain in dH₂O for 1 hr. The gels were rinsed in dH₂O containing 5% glycerol and then sandwiched between two sheets of cellophane clamped to a gel-drying apparatus and dried in a GelAir Dryer (Bio-Rad Hercules, CA). Once dry, the gels were placed in an autoradiography cassette and exposed to GE Hyperfilm MP

X-ray film overnight. The films were then developed using a Konica automatic developer. Following autoradiography, the bands corresponding to NKCC1 were excised from the dried gel, transferred to microcentrifuge tubes and ^{32}P -radioactivity incorporation was quantified by Cerenkov counting.

Small-molecule inhibitor ELISA screen—We obtained the GlaxoSmithKline published kinase inhibitor set, PKIS (Dranchak et al., 2013) to evaluate potential SPAK drug inhibitor candidates. The pilot inhibitor screen tested the capability of 320 compounds to inhibit the kinase activity of purified co-expressed $\text{S}^{\text{P}}382$ WNK1 (1-661)/ WT SPAK using an ELISA based screen monitoring a reduction in NKCC1 phosphorylation with the NKCC1 phospho-specific antibody, $\text{T}^{\text{P}}\text{NKCC1}$. 10 nL of each inhibitor compound (final concentration 20 μM) or DMSO vehicle controls were added to dry 384 well-flat bottom low volume non-binding assay plates (Corning) using an Echo 550 Acoustic dispenser (Labcyte). 125 nM SPAK (from the co-expressed variant), and 100 nM GST-NKCC1 were mixed with Kinase reaction buffer (50 mM Tris HCl pH 7.5, 150 mM NaCl, 20 mM MgCl_2 , 2 mM DTT, 0.1% BSA) that did not contain ATP, and 4 μL of the mixture was distributed into each well of the assay plate. The assay plates were centrifuged at 200 g for 1 min. then incubated at RT for 30 min. Following inhibitor incubation, the kinase reaction was initiated with 1 μL of 50 μM ATP (final concentration 10 μM) or 1 μL of Kinase reaction buffer for negative controls and reacted for 1 hr at 37°C. The reaction was then quenched with 5 μL Kinase Stop buffer (100 mM Tris pH 8, 300 mM NaCl, 40 mM EDTA) and incubated for 1 min. with shaking at 450 rpm. 2 μL of each quenched reaction was added to 18 μL TBS (50 mM Tris pH 8, 150 mM NaCl) in white 384-well Nunc Maxisorp plates (Thermo Scientific) using a PlateMate Plus (Thermo Scientific). The plate was shaken for 1 min. at 450 rpm, sealed and incubated at 4°C overnight to allow the protein contents of the reaction to bind to the Maxisorp plate. The next morning the solution was removed, and the plates were then subjected to 3 washes in TBST (50 mM Tris pH 7.5, 150 mM NaCl. 0.05% Tween 20) for 5 min each wash with shaking at 400 rpm. The plates were blocked with TBST buffer containing 3% BSA (w/v) at RT for 2 hr at RT. The blocking buffer was removed, and the plates were immunoblotted with 1:50 000 dilution of $\text{T}^{\text{P}}\text{NKCC1}$ in blocking buffer for 2 hr at RT. The plates were then subjected to 3 washes in TBST for 5 min each wash with shaking at 400 rpm, followed by incubating with 1:10 000 dilution of 2° DAR-HPR antibody in blocking buffer for 1 hr at RT. The plates were washed again 3 times in TBST for 5 min each wash with shaking at 400 rpm. Signal was detected by SuperSignal ELISA Pico Chemiluminescent substrate (Thermo Scientific) and read on an EnVision multi-label plate reader (Perkin-Elmer).

Stimulation and lysis of mDCT15—Before each set of experiments 2×10^5 mDCT15 cells/well were plated in 24-well plates treated with 100 $\mu\text{g}/\text{mL}$ poly-D-lysine and grown at 37°C in 5% CO_2 to ~95% confluency. The culture media was removed and replaced with 250 μL of pre-warmed media containing 1 μL of inhibitor compound at each specific concentration or 100% DMSO vehicle control and incubated for 2 hr at 37°C in 5% CO_2 . To stimulate hyperosmotic conditions, a 5 M NaCl stock was spiked into the media at a final concentration of 0.5 M NaCl and incubated for 10 min at 37°C in 5% CO_2 . Following the 10 min incubation the media was removed and replaced with 1 mL of hypotonic buffer

(10 mM HEPES pH 7.4, 70 mM sodium gluconate, 0.5 mM magnesium gluconate, 2.5 mM potassium gluconate, 0.5 mM calcium gluconate, 0.5 mM Na₂HPO₄, 0.5 mM NaSO₄, 5 mM dextrose), to stimulate hypo-osmotic conditions for 30 min at 37°C in 5% CO₂. All media was removed and 100 uL of cell culture lysis buffer (100 mM Tris/HCl pH 7.4, 300 mM NaCl, 5 mM EDTA, 5 mM EGTA, 2 mM DTT, 10% glycerol, 2% Triton X-100, Roche protease inhibitor, and phosphatase inhibitor cocktail 3 (Sigma-Aldrich St. Louis, MO)) was added to each well, transferred to a clean 1.5 mL Eppendorf tube, and incubated on ice for a minimum of 10 min. The cell lysates were centrifuged at 21 000 G for 10 min. The clarified lysate was stored at -80°C.

Cabozantinib (XL-184) and YU566 treatment in mDCT15—mDCT15 cells were incubated with 40 μM YU252, 40 μM Cabozantinib (XL-184), or DMSO (vehicle) for 1, 2, 3 and 4 hrs and lysed as described above for immunoblot analysis. In addition, the same conditions were applied to mDCT15 cells to perform cell imaging using bright field microscopy at 20x and 80x magnification.

Nanogrooved pattern cell migration assay: Migration of glioma cells was quantified using a directional migration assay using nano-ridges/grooves of 400 nm in groove width, 400 nm in ridge width, and 500 nm in depth, constructed of transparent poly(urethane acrylate) (PUA), and fabricated using UV-assisted capillary lithography (Kim and Eberwine, 2010). Prior to plating cells, nanogrooved substrata were coated with poly-L-ornithine (10 ug/ml concentration) for 15 minutes and laminin (10 ug/ml concentration) for 1 hour. These topographically patterned cell substrata caused cells to align with and move along the direction of the nanogrooves. Cell migration was quantified using time-lapse microscopy using a motorized inverted microscope (Olympus IX81) equipped with a Cascade 512B II CCD camera and temperature and gas controlling environmental chamber. Phase-contrast images were automatically recorded under 4*1.6X objective using the Slidebook 4.1 (Intelligent Imaging Innovations, Denver, CO) for 10 hours at 10-minute intervals. *Quantitative analysis of cell migration:* A custom-made MATLAB script was used calculate cell speed and persistence using time-lapse microscopy data as described previously (Garzon-Muvdi et al., 2012). Average speeds of individual cells were calculated from the total distance moved throughout the entire cell trajectory and the total time the cell was tracked.

Transwell migration: Transwell plates from Corning (Costar-#3422) were used to evaluate the migratory capacity of the transduced cell line in the presence and absence of the YU252 inhibitor. The concentration gradient used to ensure the migration was based on fetal bovine serum (FBS – GIBCO). Each well contained 500 uL of 2.5% FBS base media (media without any growth factors) at the bottom, and 250uL of 0.5% FBS media inside each insert. Based on optimization experiments, 30 000 cells were used per insert. The different concentrations tested for the inhibitor included 0, 5, 15, 20uM. The transwell plate was incubated for 24 hours. After the incubation, cells that remained on the upper side of the membrane were removed using a cotton swab. The membranes were stained using DAPI and visualized under the fluorescence microscope. Nine 10x-fields were captured per membrane and then analyzed to count the number of nuclei using the Arivis Vision4D software.

Cell proliferation—Glioblastoma cells were plated in triplicates in 96-well plates at a cell density of 10,000 cells per well and incubated with increasing concentrations of YU252 inhibitor for 72hs. Cell viability was determined by Thiazolyl Blue Tetrazolium Bromide (MTT) assay (Sigma) according to manufacturer instructions. IC₅₀ was determined using GraphPad software by non-linear regression analysis (log (inh) versus normalized response).

Generation of SPAK OSR1 stable double knockdowns—Plasmids containing shRNAs sequences for SPAK and OSR1 from the Sigma Mission library (PLKO) were purified from bacterial glycerol stocks (Table S2). Lentiviral particles (LVPs) were produced using a standardized protocol in the laboratory. It requires the transfection of HEK293T cells (ATCC® CRL-3216) with the transfer plasmid of interest, the packaging plasmid (psPAX2 Addgene), and the envelope vector (pMD.2 Addgene) in the presence of Lipofectamine 3000 (Thermo Scientific). The LVPs were then concentrated using Lenti-XTM Concentrator (Clontech) and resuspended in PBS for quantitative characterization by ELISA using the Lenti-X p24 Rapid Titer Kit (Takara). GBM cell 965 was transduced and selected using puromycin (Invitrogen). The knockdown efficiency was corroborated by obtaining lysates and performing WB using antibodies specific for OSR1 (Cell Signaling-#3729), SPAK (Cell Signaling-#2281).

Bioluminescence imaging—*In vivo* bioluminescence images of tumor-implanted mice were obtained using the IVIS Spectrum System. Before imaging, D-luciferin (XenoLight D-Luciferin - K+ Salt Bioluminescent Substrate Perkin Elmer) was injected I.P., at a dose of 10 mg/kg and allowed to distribute for 10 min. Mice were imaged once a week after tumor engrafting. Data acquisition and analysis were performed using the Living Image Software. For quantitation of the detected light, regions of interest were drawn, and the light emitted was recorded as the total flux (number of photons per second).

QUANTIFICATION AND STATISTICAL ANALYSIS

Statistical analysis was performed using GraphPad Prism 8 by Wilcoxon rank-sum test. Non-linear regression exponential growth equation was used to determine BLI tumor growth dynamics.

An α -level of 0.05 was established to determine statistical significance.

Supplementary Material

Refer to Web version on PubMed Central for supplementary material.

ACKNOWLEDGMENTS

We are grateful to the members of the Rinehart, Isaacs, Levchenko, and Quiñones-Hinojosa labs for critical review and comments during manuscript preparation. We would like to thank the following individuals for access to valuable tools and reagents: William Zuercher (access to PKIS), Joerg Nikolaus (imaging), David Campbell (mass spectrometry), Biff Forbush (antibodies), Visar Ajeti and Mike Murrell (cell volume imaging), and Dario Alessi. J.R. and F.J.I. are supported by the NIH (GM117230, CA209992). A.L. is supported by the NIH (CA209992). A.Q.-H. is supported by the NIH (CA200399). P.S. is supported by the Georg Haub Career Development Award in Cancer Research Honoring Richard F. Emslander.

REFERENCES

- AlAmri MA, Kadri H, Alderwick LJ, Simpkins NS, and Mehellou Y (2017). Rafoxanide and closantel inhibit SPAK and OSR1 kinases by binding to a highly conserved allosteric site on their C-terminal domains. *ChemMed-Chem* 12, 639–645.
- Barber KW, and Rinehart J (2018). The ABCs of PTMs. *Nat. Chem. Biol* 14, 188–192. [PubMed: 29443972]
- Chiu MH, Liu HS, Wu YH, Shen MR, and Chou CY (2014). SPAK mediates KCC3-enhanced cervical cancer tumorigenesis. *FEBS J.* 281, 2353–2365. [PubMed: 24655550]
- Cuddapah VA, and Sontheimer H (2011). Ion channels and transporters [corrected] in cancer. 2. Ion channels and the control of cancer cell migration. *Am. J. Physiol. Cell Physiol* 301, C541–C549. [PubMed: 21543740]
- Delpire E, and Gagnon KB (2008). SPAK and OSR1: STE20 kinases involved in the regulation of ion homeostasis and volume control in mammalian cells. *Biochem. J* 409, 321–331. [PubMed: 18092945]
- Dowd BFX, and Forbush B (2003). PASK (proline-alanine-rich STE20-related kinase), a regulatory kinase of the Na-K-Cl cotransporter (NKCC1). *J. Biol. Chem* 278, 27347–27353. [PubMed: 12740379]
- Dranchak P, MacArthur R, Guha R, Zuercher WJ, Drewry DH, Auld DS, and Inglese J (2013). Profile of the GSK published protein kinase inhibitor set across ATP-dependent and-independent luciferases: Implications for reporter-gene assays. *PLoS ONE* 8, e57888. [PubMed: 23505445]
- Filippi BM, de los Heros P, Mehellou Y, Navratilova I, Gourlay R, Deak M, Plater L, Toth R, Zeqiraj E, and Alessi DR (2011). MO25 is a master regulator of SPAK/OSR1 and MST3/MST4/YSK1 protein kinases. *EMBO J.* 30, 1730–1741. [PubMed: 21423148]
- Flemmer AW, Gimenez I, Dowd BFX, Darman RB, and Forbush B (2002). Activation of the Na-K-Cl cotransporter NKCC1 detected with a phospho-specific antibody. *J. Biol. Chem* 277, 37551–37558. [PubMed: 12145305]
- Galli R, Binda E, Orfanelli U, Cipelletti B, Gritti A, DeVitis S, Fiocco R, Foroni C, Dimeco F, and Vescovi A (2004). Isolation and characterization of tumorigenic, stem-like neural precursors from human glioblastoma. *Cancer Res.* 64, 7011–7021. [PubMed: 15466194]
- Garzon-Muvdi T, Schiapparelli P, ap Rhys C, Guerrero-Cazares H, Smith C, Kim DH, Kone L, Farber H, Lee DY, An SS, et al. (2012). Regulation of brain tumor dispersal by NKCC1 through a novel role in focal adhesion regulation. *PLoS Biol.* 10, e1001320. [PubMed: 22570591]
- Giménez I (2006). Molecular mechanisms and regulation of furosemide-sensitive Na-K-Cl cotransporters. *Curr. Opin. Nephrol. Hypertens* 15, 517–523. [PubMed: 16914965]
- Grimm PR, Taneja TK, Liu J, Coleman R, Chen YY, Delpire E, Wade JB, and Welling PA (2012). SPAK isoforms and OSR1 regulate sodium chloride co-transporters in a nephron-specific manner. *J. Biol. Chem* 287, 37673–37690. [PubMed: 22977235]
- Haas BR, Cuddapah VA, Watkins S, Rohn KJ, Dy TE, and Sontheimer H (2011). With-no-lysine kinase 3 (WNK3) stimulates glioma invasion by regulating cell volume. *Am. J. Physiol. Cell Physiol* 301, C1150–C1160. [PubMed: 21813709]
- Hutti JE, Jarrell ET, Chang JD, Abbott DW, Storz P, Toker A, Cantley LC, and Turk BE (2004). A rapid method for determining protein kinase phosphorylation specificity. *Nat. Methods* 1, 27–29. [PubMed: 15782149]
- Isaacs FJ, Carr PA, Wang HH, Lajoie MJ, Sterling B, Kraal L, Tolonen AC, Gianoulis TA, Goodman DB, Reppas NB, et al. (2011). Precise manipulation of chromosomes in vivo enables genome-wide codon replacement. *Science* 333, 348–353. [PubMed: 21764749]
- Kikuchi E, Mori T, Zeniya M, Isobe K, Ishigami-Yuasa M, Fujii S, Kagechika H, Ishihara T, Mizushima T, Sasaki S, et al. (2015). Discovery of novel SPAK inhibitors that block WNK kinase signaling to cation chloride transporters. *J. Am. Soc. Nephrol* 26, 1525–1536. [PubMed: 25377078]
- Kim TK, and Eberwine JH (2010). Mammalian cell transfection: The present and the future. *Anal. Bioanal. Chem* 397, 3173–3178. [PubMed: 20549496]

- Köchl R, Thelen F, Vanes L, Brazão TF, Fountain K, Xie J, Huang CL, Lyck R, Stein JV, and Tybulewicz VL (2016). WNK1 kinase balances T cell adhesion versus migration in vivo. *Nat. Immunol* 17, 1075–1083. [PubMed: 27400149]
- Lajoie MJ, Rovner AJ, Goodman DB, Aerni HR, Haimovich AD, Kuznetsov G, Mercer JA, Wang HH, Carr PA, Mosberg JA, et al. (2013). Genomically recoded organisms expand biological functions. *Science* 342, 357–360. [PubMed: 24136966]
- Miller CJ, and Turk BE (2016). Rapid identification of protein kinase phosphorylation site motifs using combinatorial peptide libraries. *Methods Mol. Biol* 1360,203–216. [PubMed: 26501912]
- Miller ML, Jensen LJ, Diella F, Jørgensen C, Tinti M, Li L, Hsiung M, Parker SA, Bordeaux J, Sicheritz-Ponten T, et al. (2008). Linear motif atlas for phosphorylation-dependent signaling. *Sci. Signal* 1, ra2. [PubMed: 18765831]
- Mok J, Kim PM, Lam HYK, Piccirillo S, Zhou X, Jeschke GR, Sheridan DL, Parker SA, Desai V, Jwa M, et al. (2010). Deciphering protein kinase specificity through large-scale analysis of yeast phosphorylation site motifs. *Sci. Signal* 3, ra12. [PubMed: 20159853]
- Moriguchi T, Urushiyama S, Hisamoto N, Iemura S, Uchida S, Natsume T, Matsumoto K, and Shibuya H (2005). WNK1 regulates phosphorylation of cation-chloride-coupled cotransporters via the STE20-related kinases, SPAK and OSR1. *J. Biol. Chem* 280, 42685–42693. [PubMed: 16263722]
- Naguro I, Umeda T, Kobayashi Y, Maruyama J, Hattori K, Shimizu Y, Kataoka K, Kim-Mitsuyama S, Uchida S, Vandewalle A, et al. (2012). ASK3 responds to osmotic stress and regulates blood pressure by suppressing WNK1-SPAK/OSR1 signaling in the kidney. *Nat. Commun* 3, 1285. [PubMed: 23250415]
- Needham EJ, Parker BL, Burykin T, James DE, and Humphrey SJ (2019). Illuminating the dark phosphoproteome. *Sci. Signal* 12, eaau8645. [PubMed: 30670635]
- Park HS, Hohn MJ, Umehara T, Guo LT, Osborne EM, Benner J, Noren CJ, Rinehart J, and Söll D (2011). Expanding the genetic code of *Escherichia coli* with phosphoserine. *Science* 333, 1151–1154. [PubMed: 21868676]
- Piechotta K, and Delpire E (2002). Characterization of the interaction between cation-chloride cotransporters and tire stress-activated serine-threonine-kinases SPAK and OSR1. *FASEB J.* 16, A57–A58.
- Pirman NL, Barber KW, Aerni HR, Ma NJ, Haimovich AD, Rogulina S, Isaacs FJ, and Rinehart J (2015). A flexible codon in genomically recoded *Escherichia coli* permits programmable protein phosphorylation. *Nat. Commun* 6, 8130. [PubMed: 26350500]
- Rafiqi FH, Zuber AM, Glover M, Richardson C, Fleming S, Jovanovi S, Jovanovi A, O’Shaughnessy KM, and Alessi DR (2010). Role of the WNK-activated SPAK kinase in regulating blood pressure. *EMBO Mol. Med* 2, 63–75. [PubMed: 20091762]
- Richardson C, and Alessi DR (2008). The regulation of salt transport and blood pressure by the WNK-SPAK/OSR1 signalling pathway. *J. Cell Sci* 121, 3293–3304. [PubMed: 18843116]
- Rinehart J, Maksimova YD, Tanis JE, Stone KL, Hodson CA, Zhang J, Risinger M, Pan W, Wu D, Colangelo CM, et al. (2009). Sites of regulated phosphorylation that control K-Cl cotransporter activity. *Cell* 138, 525–536. [PubMed: 19665974]
- Schiapparelli P, Guerrero-Cazares H, Magaña-Maldonado R, Hamilla SM, Ganaha S, Goulin Lippi Fernandes E, Huang CH, Aranda-Espinoza H, Devreotes P, and Quinones-Hinojosa A (2017). NKCC1 regulates migration ability of glioblastoma cells by modulation of actin dynamics and interacting with Cofilin. *EBioMedicine* 21, 94–103. [PubMed: 28679472]
- Sie ZL, Li RY, Sampurna BP, Hsu PJ, Liu SC, Wang HD, Huang CL, and Yuh CH (2020). WNK1 kinase stimulates angiogenesis to promote tumor growth and metastasis. *Cancers (Basel)* 12, 575.
- Smith CL, Kilic O, Schiapparelli P, Guerrero-Cazares H, Kim DH, Sedora-Roman NI, Gupta S, O’Donnell T, Chaichana KL, Rodriguez FJ, et al. (2016). Migration phenotype of brain-cancer cells predicts patient outcomes. *Cell Rep.* 15, 2616–2624. [PubMed: 27292647]
- Szewczuk LM, Tarrant MK, and Cole PA (2009). Protein phosphorylation by semisynthesis: From paper to practice. *Methods Enzymol.* 462, 1–24. [PubMed: 19632467]
- Thastrup JO, Rafiqi FH, Vitari AC, Pozo-Guisado E, Deak M, Mehellou Y, and Alessi DR (2012). SPAK/OSR1 regulate NKCC1 and WNK activity: Analysis of WNK isoform interactions and activation by T-looptrans-autophosphorylation. *Biochem. J* 441, 325–337. [PubMed: 22032326]

- Vitari AC, Deak M, Morrice NA, and Alessi DR (2005). The WNK1 and WNK4 protein kinases that are mutated in Gordon's hypertension syndrome phosphorylate and activate SPAK and OSR1 protein kinases. *Biochem. J* 331, 17–24.
- Vitari AC, Thastrup J, Rafiqi FH, Deak M, Morrice NA, Karlsson HK, and Alessi DR (2006). Functional interactions of the SPAK/OSR1 kinases with their upstream activator WNK1 and downstream substrate NKCC1. *Biochem. J* 337, 223–231.
- Wilson FH, Disse-Nicodème S, Choate KA, Ishikawa K, Nelson-Williams C, Desitter I, Gunel M, Milford DV, Lipkin GW, Achard JM, et al. (2001). Human hypertension caused by mutations in WNK kinases. *Science* 293, 1107–1112. [PubMed: 11498583]
- Workman CT, Yin Y, Corcoran DL, Ideker T, Stormo GD, and Benos PV (2005). enoLOGOS: A versatile web tool for energy normalized sequence logos. *Nucleic Acids Res.* 33, W389–92. [PubMed: 15980495]
- Xu BE, Min X, Stippec S, Lee BH, Goldsmith EJ, and Cobb MH (2002). Regulation of WNK1 by an autoinhibitory domain and autophosphorylation. *J. Biol. Chem* 277, 48456–48462. [PubMed: 12374799]
- Yamada K, Park HM, Rigel DF, DiPetrillo K, Whalen EJ, Anisowicz A, Beil M, Berstler J, Brocklehurst CE, Burdick DA, et al. (2016). Small-molecule WNK inhibition regulates cardiovascular and renal function. *Nat. Chem. Biol* 12, 896–898. [PubMed: 27595330]
- Zagórska A, Pozo-Guisado E, Boudeau J, Vitari AC, Rafiqi FH, Thastrup J, Deak M, Campbell DG, Morrice NA, Prescott AR, and Alessi DR (2007). Regulation of activity and localization of the WNK1 protein kinase by hyperosmotic stress. *J. Cell Biol* 176, 89–100. [PubMed: 17190791]
- Zhu W, Begum G, Pointer K, Clark PA, Yang SS, Lin SH, Kahle KT, Kuo JS, and Sun D (2014). WNK1-OSR1 kinase-mediated phospho-activation of Na⁺-K⁺-2Cl⁻ cotransporter facilitates glioma migration. *Mol. Cancer* 13, 31. [PubMed: 24555568]

Highlights

- Bacterial strain with expanded genetic code incorporates phosphoserine into WNK1
- Synthetically phosphorylated WNK1 activates SPAK and enables substrate discovery
- Active WNK1/SPAK pathway yields a screen for small-molecule kinase inhibitors
- Inhibitors modulate WNK/SPAK control of cell volume and reduce GBM migration

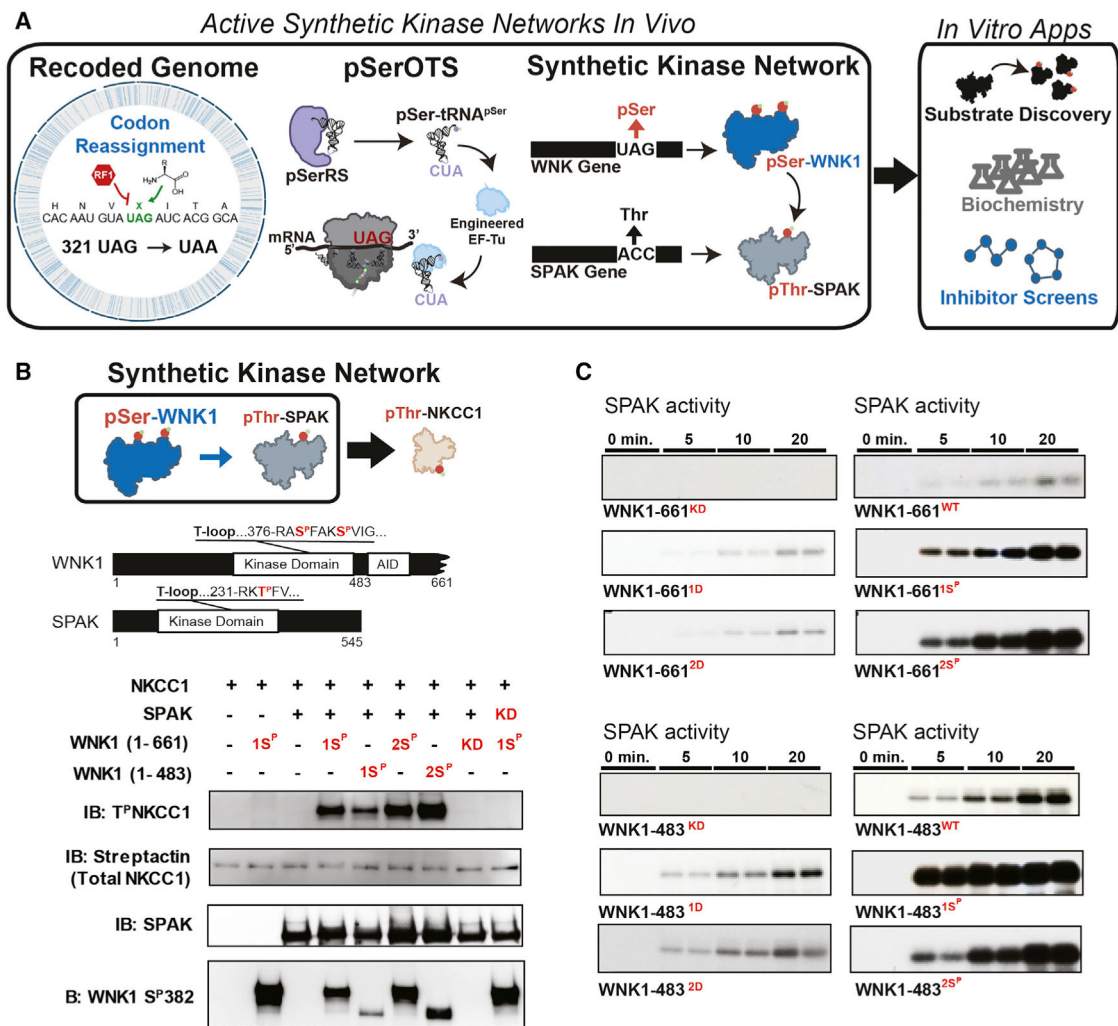


Figure 1. A synthetic kinase network activated by WNK1 containing genetically encoded phosphoserine

(A) Synthetic kinase networks are expressed in a bacterial cell with a recoded genome. Codon reassignment enables genetically encoded phosphoserine at UAG codons. The phosphoserine orthogonal translation system (pSerOTS) contains a pSerRS that charges phosphoserine onto tRNA^{pSer} and directs phosphoserine incorporation at UAG codons in the ribosome. WNK1 is activated by genetically encoded phosphoserine S382 and S378/S382 and phosphorylates SPAK on an activating threonine residue (T233).

(B) The synthetic WNK/SPAK kinase network phosphorylates NKCC1 *in vitro*. The activating T-loop phosphorylation sites for each kinase are highlighted in red. WNK1 variants (with and without the autoinhibitory domain [AID]) and SPAK were co-expressed and kinase activity was tested with an NKCC1 substrate *in vitro*. Kinase activity was monitored by immunoblotting (IB) with antibody recognizing phosphorylated NKCC1 (T^PNKCC1), total NKCC1 (StrepTactin IB), SPAK, and phosphorylated WNK1 (SP382).

(C) NKCC1 phosphorylation was monitored by ³²P autoradiography in kinase reactions containing SPAK, MO25 α , and the WNK1 variants listed (KD, kinase dead; WT, serine; S^P, genetically encoded phosphoserine; D, aspartate for serine substitution).

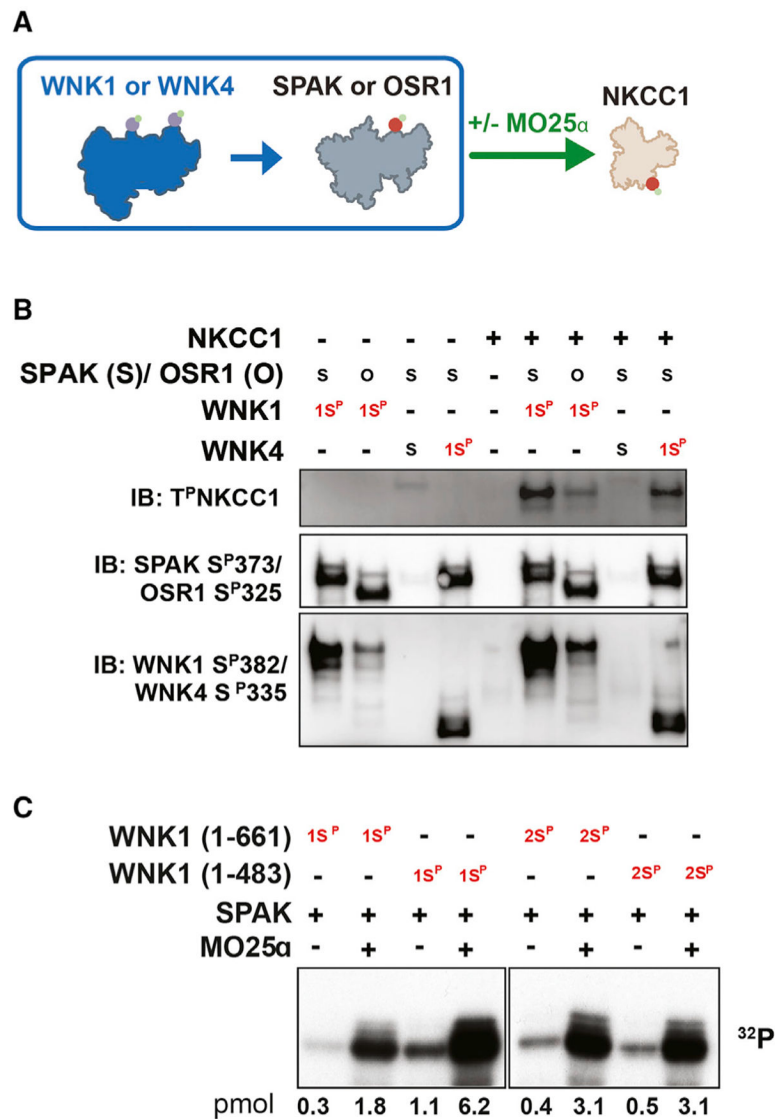


Figure 2. The synthetic kinase network is amenable to multiple kinase combinations and responsive to cofactors

(A) Genetically encoded phosphoserine in WNK1 or WNK4 phosphorylating SPAK or OSR1 in the presence or absence of MO25α and subsequent phosphorylation of NKCC1.

(B) NKCC1 phosphorylation was monitored by IB to assess the activities of the WNK1/WNK4/OSR1/SPAK combinations shown. WNK4 activation was compared with serine (S) or phosphoserine (S^P) encoded in its T-loop. SPAK/OSR1 phosphorylation (SPAK S^P373 or OSR1 S^P325) and WNK1/WNK4 phosphorylation (WNK1 S^P382 or WNK4 S^P335) was monitored by IB.

(C) NKCC1 phosphorylation was monitored by ³²P autoradiography in kinase reactions containing combinations of WNK1 (with and without the AID), SPAK, and MO25α.

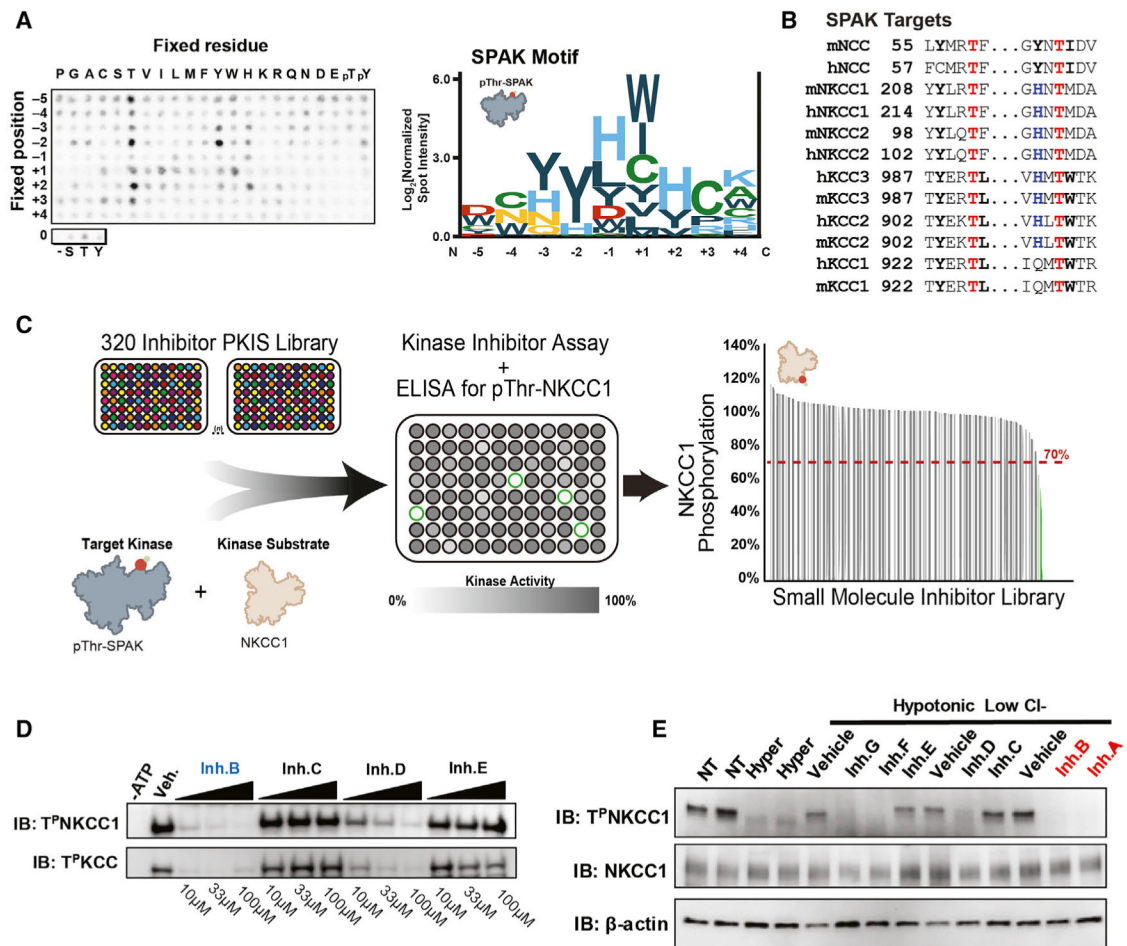


Figure 3. Substrate motif characterization and small-molecule inhibitor screens with the synthetic WNK/SPAK kinase network

(A) SPAK kinase motif characterization using the positional scanning peptide library (PSPL) bearing the denoted amino acid at defined positions relative to a central S/T phospho-acceptor site (left panel). SPAK kinase motif sequence logo (right panel) representing the amino acid preferences at different positions relative to the phosphorylation site was derived from the PSPL data.

(B) Sequence alignment of ion co-transporters regulated by SPAK phosphorylation *in vivo*. Amino acids are highlighted to match sequence elements in the PSPL motif data, with phosphorylated threonine residues highlighted in red.

(C) 320 compounds from the GSK published inhibitor set (PKIS) were evaluated for SPAK inhibition with an *in vitro* ELISA screen for SPAK-dependent NKCC1 phosphorylation. Phosphorylated, active SPAK was purified from the synthetic kinase network and kinase activity was monitored with a phospho-specific antibody for pThr-NKCC1. Seven hits were identified that showed reduction in NKCC1 phosphorylation ranging from 34% to 58% at inhibitor concentrations of 27 μ M.

(D) A subset of the hits from the ELISA screen were further evaluated using both NKCC1 and KCC (SPAK substrates), varying inhibitor doses, and immunoblotting with T^pNKCC1 and T^pKCC.

(E) Hit validation performed in mDCT15 cells incubated with the seven compounds (Inh. A–G). NKCC1 phosphorylation was measured using a T^PNKCC1 and β -actin.

Author Manuscript

Author Manuscript

Author Manuscript

Author Manuscript

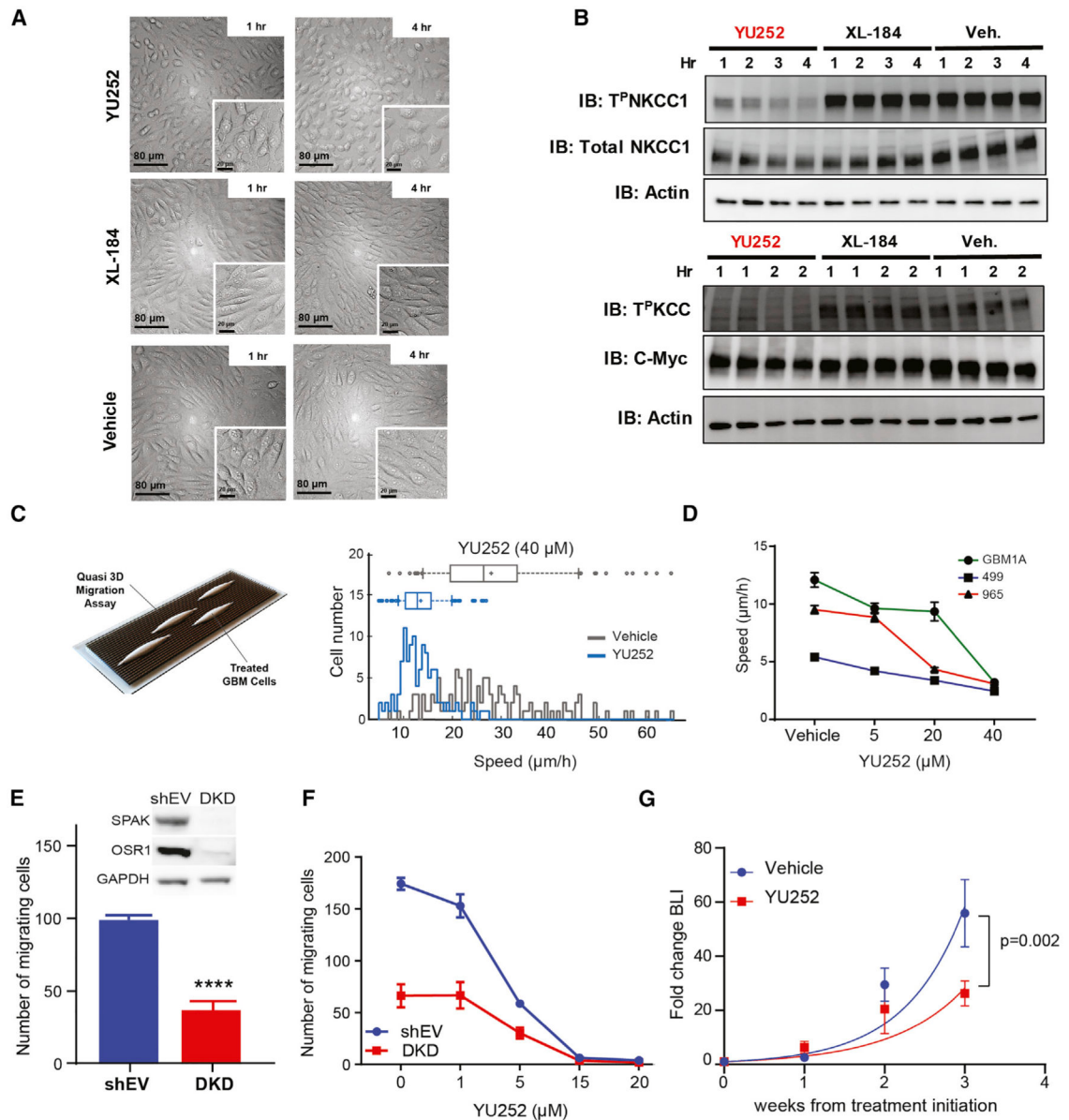


Figure 4. Cellular characterization of the SPAK inhibitor YU252

(A) mDCT15 cells were incubated with YU252, cabozantinib (XL-184), or DMSO (vehicle) and imaged using bright-field microscopy.

(B) Time-course analysis of mDCT15 cells treated with YU252, XL-184, or vehicle; phosphorylation was measured using T^PNKCC1 and NKCC1 (upper panel). HEK293 overexpressing myc-tagged KCCs were incubated with YU252, XL-184, or vehicle. KCC phosphorylation was measured using a T^PKCC and total KCC antibody (c-Myc).

(C) Schematic representation of migration assay using a tissue-mimetic nanopatterned substrate. Histograms and boxplots show cell distribution with respect to average migration speed for GBM499 cells treated with YU252 compared to vehicle control.

(D) Comparison of average migration speed of GBM cell lines 499, 965, and GBM1A cells treated with YU252 compared to the equivalent DMSO vehicle control.

(E) Cell migration analysis of SPAK and OSR1 double knockdown (DKD) cells and control GBM cells (shEV). Western blot of OSR1 and SPAK in DKD and shEV (inset).

(F) Cell migration analysis of SPAK and OSR1 DKD and control cells treated with increasing doses of YU252 inhibitor.

(G) Tumor growth inhibition in athymic mice in response to daily intraperitoneal injections of YU252 (n = 5). Data are represented as mean \pm SEM. ****p > 0.001.

Author Manuscript

Author Manuscript

Author Manuscript

Author Manuscript

KEY RESOURCES TABLE

REAGENT or RESOURCE	SOURCE	IDENTIFIER
Antibodies		
Rabbit polyclonal anti-OSR1	cell signaling	Cat#3729; RRID: AB_2157610
Rabbit polyclonal anti-SPAK	cell signaling	Cat#2281; RRID: AB_2196951
Sheep polyclonal anti-SPAK	Division of Signal Transduction (DSTT), Dundee	N/A
Rabbit monoclonal anti-NKCC1 (T4)	Biff Forbush, Yale University	T4 was deposited to the DSHB by Lytle, C. and Forbush III, B. (DSHB Hybridoma Product T4)
Rabbit polyclonal anti-WNK1 S ^P 382	Richard Lifton, Yale University	N/A
Rabbit polyclonal anti-T ^P NKCC1 (R5)	Biff Forbush, Yale University J Biol Chem 2002 Oct 4;277(40):37551-8. https://doi.org/10.1074/jbc.M206294200 . Epub 2002 Jul 26.	Biff Forbush, Yale University
Strep-Tactin® conjugate	Iba-Life sciences	Cat#2-1502-001
Donkey Anti-Rabbit-HRP	Jackson ImmunoResearch	Cat#711-035-152
Donkey Anti-Sheep HRP	Jackson ImmunoResearch	Cat#713-035-147
Bacterial and virus strains		
EcAR7	Addgene	Cat#52055; RRID: Addgene_52055
Lentiviral particles (LVP)	Produced in Quinones-Hinojosa's laboratory. Mayo Clinic FL	N/A
Chemicals, peptides, and recombinant proteins		
GST-Prescission™ protease	GE Healthcare (now Cytiva)	Cat#27084301
epidermal growth factor (EGF)	PeproTech	Cat#AF-100-15
fibroblast-derived growth factor	PeproTech	Cat#AF-100-18B
R&D Systems Cultrex Mouse Laminin I Pathclear	R&D Systems	Cat#34-000-1002
YU252	This paper	N/A
Kinase Substrates Library, Groups I and II	Anaspec, Inc (Mok et al., 2010)	N/A
Kinase inhibitor set, PKIS	GlaxoSmithKline (Dranchak et al., 2013)	N/A
Critical commercial assays		
Thiazolyl Blue Tetrazolium Bromide (MTT) assay	Sigma	Cat#M5655
Lenti-X p24 Rapid Titer Kit	Takara	Cat#632200
Experimental models: Cell lines		
Mouse distal convoluted tubule (mDCT15)	Robert Hoover, Emory	N/A
Human embryonic kidney HEK293T	ATCC	Cat#CRL-3216; RRID: CVCL_0063
Primary-derived human Glioblastoma cell lines: GBM499, GBM640, GBM612, GBM965 and GBM1A	Quinones-Hinojosa laboratory, Mayo Clinic Jacksonville	N/A
Experimental models: Organisms/strains		
male athymic nude Foxn1nu	Jackson Laboratories	Cat#007850
Recombinant DNA		
psPAX2	Addgene	Cat#12260; RRID: Addgene_12260
pMD.2	Addgene	Cat#12259; RRID: Addgene_12259

REAGENT or RESOURCE	SOURCE	IDENTIFIER
WT-WNK1 (DU6025)	Division of Signal Transduction (DSTT), Dundee	N/A
WT-SPAK (DU6040)	Division of Signal Transduction (DSTT), Dundee	N/A
Kinase Dead D212A-HA SPAK (DU6013),	Division of Signal Transduction (DSTT), Dundee	N/A
WTOSR1 (DU41905)	Division of Signal Transduction (DSTT), Dundee	N/A
WT-MO25 α (DU2945)	Division of Signal Transduction (DSTT), Dundee	N/A
pGEX-6P-1	Division of Signal Transduction (DSTT), Dundee	N/A
pSerOTS	Jesse Rinehart. Yale University	N/A
N-terminal Strep-tagged human NKCC1	Jesse Rinehart. Yale University	N/A
Software and algorithms		
GraphPad Prism 9	GraphPad Software, Inc, USA	https://www.graphpad.com/scientific-software/prism/
Arivis Vision4D	arivis AG, USA	https://imaging.arivis.com/en/imaging-science/arivis-vision4d
MATLAB	The MathWorks, Inc.	https://www.mathworks.com/products/matlab.html
enoLOGOS	National Science Foundation	http://www.benoslab.pitt.edu/cgi-bin/enologos/enologos.cgi
Biorender	©BioRender 2021	https://biorender.com/